

Improved proton-transfer barriers with van der Waals density functionals: Role of repulsive non-local correlation

S. Seyedraoufi¹ and Kristian Berland^{1,*}

¹*Department of Mechanical Engineering and Technology Management, Norwegian University of Life Sciences, Norway.*

(Dated: April 11, 2022)

Proton-transfer (PT) between organic complexes is a common and important biochemical process. Unfortunately, PT energy barriers are difficult to accurately predict using density functional theory (DFT); in particular, the generalized gradient approximation (GGA) tends to underestimate PT barriers. Moreover, PT typically occurs in environments where dispersion forces contribute to the cohesion of the system; thus, a suitable exchange-correlation functional should accurately describe both dispersion forces and PT barriers. This paper provides benchmark results for the PT barriers of several density functionals including several variants of the van der Waals density functional (vdW-DF). The benchmark set comprises small organic molecules with inter- and intra-molecular PT. The results show that replacing GGA correlation with a fully non-local vdW-DF correlation increases the PT barriers, making it closer to the quantum chemical reference values. In contrast, including non-local correlations with the Vydrov-Voorhis (VV) method or dispersion-corrections at the DFT-D3 or the Tkatchenko-Scheffler (TS) level has barely any impact on the PT barriers. Hybrid functionals also increase and improve the energies and the best performance is provided by a hybrid version of the consistent-exchange van der Waals density functional vdW-DF-cx. For the formic acid dimer PT system, we analyzed the GGA exchange and non-local correlation contributions. The analysis shows that the repulsive part of the non-local correlation kernel plays a key role in the PT energy barriers predicted with vdW-DF.

I. INTRODUCTION

Proton transfer (PT) is an ubiquitous chemical reaction and many biochemical reactions involve PT. For instance, proton-coupled charge transfer is an established mechanism in enzymology³ and collective proton transfer in DNA base pairs can give rise to rare tautomers which may lead to mutations.⁴ In organic solid-state systems, PT can change the nature of the bonding and, consequently, the properties of a crystal.⁵ PT is also one mechanism for electric polarization switching in the organic ferroelectrics.^{6–8}

High level quantum chemical methods, in particular, coupled-cluster with single and double and perturbative triple excitations (CCSD(T)) can provide accurate reference data for PT energy barriers, but its high computational cost makes it ill-suited for complex PT systems. The organic complexes in which PT occurs are often held together by van der Waals forces, making it important to assess the accuracy of predicted PT barriers with functionals that include dispersion forces.

Earlier benchmark studies have found that density functional theory (DFT) in the local density approximation (LDA)⁹ and generalized-gradient approximation (GGA)^{10,11} tend to underestimate PT barriers.^{1,12} Hybrid functionals, which mix in a fraction of Fock exchange,^{13–16} improve performance¹ which, in part, can be linked to reduced self-interaction error.¹⁷ Patchkovskii et al.¹⁸ found that Perdew-Zunger self-interaction corrected DFT improves reaction and activation energy barriers for 11 selected “difficult” reactions compared to

LDA and GGA. Although self interaction is one source of the PT barrier underestimation, lack of non-local correlation effects has also been suggested as a possible source of inaccuracy.¹⁹

Several different methods for including dispersion forces in DFT have been developed, but most of these use “dispersion correction” scheme in which van der Waals forces are reintroduced with atomistic force-field correction.^{20–25} One class of functionals^{26–35} with a non-local account of the correlation is the Chalmers-Rutgers van der Waals (vdW-DF) density functional^{26,34,36} which is a popular method to describe materials bonded by dispersion forces. vdW-DF is derived from exact criteria using a plasmon-model of the response properties of the electron-gas.^{26,30,35–38} In the theory, the non-local correlation energy takes the form,

$$E_c^{\text{nl}}[n] = \frac{1}{2} \int d^3\mathbf{r}_1 \int d^3\mathbf{r}_2 n(\mathbf{r}_1) \phi(\mathbf{r}_1, \mathbf{r}_2) n(\mathbf{r}_2), \quad (1)$$

in which a kernel function $\phi(\mathbf{r}_1, \mathbf{r}_2)$ connects two density regions $n(\mathbf{r}_1)$ and $n(\mathbf{r}_2)$. Unlike other dispersion-correction methods, vdW-DF is designed so that E_c^{nl} vanishes seamlessly into a homogeneous electron gas limit without the inclusion of damping terms. Therefore, vdW-DF does not include gradient components of the GGA correlation in the total exchange-correlation energy, i.e. $E_{xc}[n] = E_x^{\text{GGA}}[n] + E_c^{\text{LDA}}[n] + E_c^{\text{nl}}[n]$. Over the years, several variants of vdW-DF^{26–28,30–33,39} have been developed including hybrid variants.^{40,41} vdW-DF has also inspired other non-local correlation functionals; in particular the Vydrov-Voorhis (VV10)⁴² functional and its revision for planewave codes (rVV10).⁴³ While vdW-DF is foremost developed for describing dispersion-bonded systems, its explicit non-local corre-

* E-mail: kristian.berland@nmbu.no

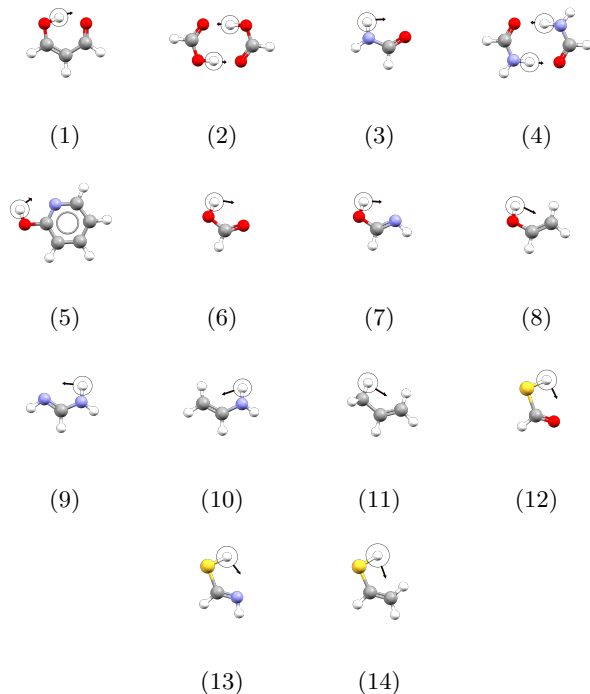


FIG. 1: Structures of the PT14 benchmark set. Arrows indicate the direction of proton transfers. Reaction systems comprise: (1) malonaldehyde, (2) formic acid dimer, (3) formamide, (4) formamide dimer, (5) pyridine, and nine tautomerization reactions including (6-8) carbonyls, (9-10) imines, (11) propene, and (12-14) thiocarbonyls. Color scheme: O (red), C (grey), H (white), N (blue), S (yellow).

lation has also been found to improve various material properties^{28,30,37,44} including image plane states on graphene.⁴⁵

This paper provides benchmark results for 22 different functionals including a number of vdW-DFs. The benchmark set labelled PT14 is based on the 9 charge-neutral intra-molecular PT systems by Karton et al.² and 5 inter- and intra-molecular PT systems by Mangiatordi et al.¹ computed with coupled-cluster method at the CCSD(T) level of theory. The set of systems are displayed in Fig. 1. In addition to vdW-DFs, we tested several GGAs,^{46,47} two standard hybrid functionals,^{15,16} and the strongly constrained and appropriately normed (SCAN) meta-GGA functional.⁴⁸ We also tested the rVV10 variant^{42,43} as well as the SCAN-rVV10 functional.⁴⁹ Moreover, for several of the GGAs, we tested the effect of adding force-field dispersion corrections at the D3²³ and Tkatchenko-Scheffler (TS)²⁰ level of theory.

We found, as detailed in Sec. III, that vdW-DF tends to increase PT barriers compared to GGA and therefore reduce the deviation with the reference data, in particular if the exchange functional is kept fixed. This trend was found to arise from a reduction in the negative correlation contribution to the PT barriers. To gain better

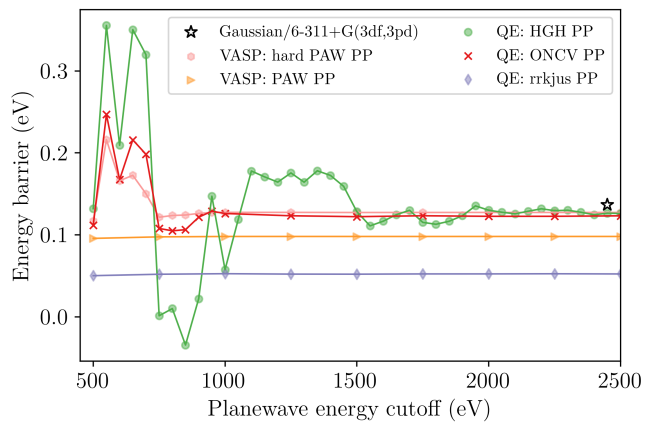


FIG. 2: PT energy barrier sensitivity of the formic acid dimer to planewave energy cutoff for different PPs. The black star indicates the energy barrier of Mangiatordi et al.¹ study using a 6-311+G(3df,3pd) orbital basis.

understanding of this result, we performed an in-depth analysis of the case of formic acid dimer (system 2 in Fig. 1), as detailed in Sec. IV. The non-local correlation contribution was analyzed and found to be linked to repulsive short-range non-local correlation effects. This effect is similar to that of GGA-type correlation but with the local geometry-sensitivity inherited to vdW-DF.

II. METHODS

The benchmark calculations were carried out with the VASP software package,⁵⁰⁻⁵² except for the vdW-DF3-opt1, vdW-DF3-opt2,³³ and B3LYP(-D3)¹⁶ calculations for which QUANTUM ESPRESSO^{53,54} was used, as these functionals are only implemented in the latter. In the supercells, 15 Å vacuum padding was used to isolate the molecular systems employing the dipole correction scheme of Neugebauer et al.⁵⁵ The electronic self-consistency criteria was set to 10^{-6} eV. The plane-wave energy cutoff was set to 1000 eV based on our convergence study as detailed in the next section. The VASP calculations used hard projected augmented waves (PAW) pseudopotentials (PPs) while the QUANTUM ESPRESSO used the recently developed optimized norm-conserving Vanderbilt (ONCV).⁵⁶ For the exchange and correlation analysis, we obtained input data from the recently developed PPACF post-processing tool⁵⁷ which is distributed as part of the QUANTUM ESPRESSO software package.

A. Pseudopotential choice and convergence

In the energy cutoff convergence study and PP selection, we compared the ultra-soft Rappe-Rabe-Kaxiras-Joannopoulos (RRKJUS) pseudopotential,⁵⁸ the

hard norm-conserving PP Hartwigsen–Goedecker–Hutter (HGh),⁵⁹ and the recently developed ONCV as implemented in QUANTUM ESPRESSO as well as the standard and hard PAW PP^{60,61} as implemented in VASP.

Fig. 2 displays the results for the case of PT barriers of the formic acid dimer. It shows that while ONCV, HGh, and hard PAW converge to a similar value of 0.12 eV, this value differs from the converged value of the ultrasoft RRKJUS and standard PAW, by 0.07 eV and 0.03 eV, respectively. In comparison, the literature value obtained with 6-311+G(3df,3pd) orbital basis set using GAUSSIAN program package⁶² is 0.13 eV.¹ The similarity of the ONCV, HGh, and hard PAW results demonstrates the reliability of these PPs. Our results are in line with the fact that ONCV has been shown to perform well compared to all-electron results for a selected set of solids including covalent, ionic, and metallic bonding.⁵⁶ In contrast to ONCV and hard PW which converge smoothly to within 1 meV at 1000 eV, the PT barriers obtained with HGh fluctuates significantly with the cutoff until the energy differences fall within 1 meV at an energy cutoff of 2800 eV.

III. RESULTS

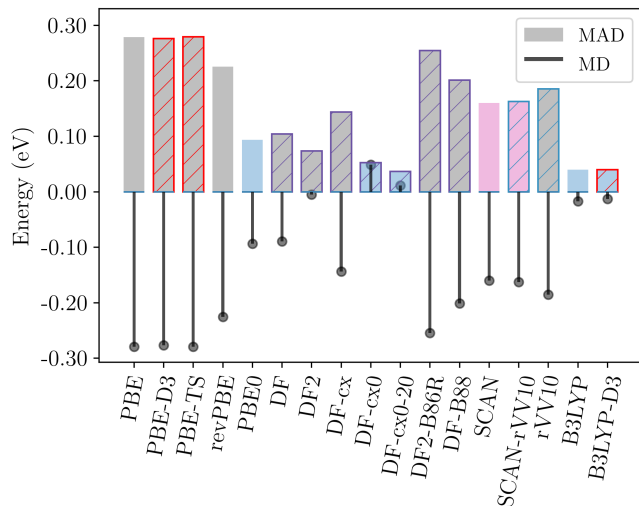


FIG. 3: Mean (absolute) deviation (M(A)D) for PT barrier energies of the PT14 benchmarking set. The bar colors indicate the nature of the respective exchange functionals, with GGAs indicated in gray, hybrids in blue, and meta-GGAs in pink. Stripes indicate the inclusion of dispersion forces, either with a dispersion correction (red stripes), or using full non-local correlation within vdW-DF (indigo) or at the rVV10 (light blue) level. (“vdW-” is dropped in the functional names).

Fig. 3 displays computed statistical data for PT barrier energies for the PT14 set for a subset of the bench-

marked functionals. The full set of results are provided in Tab. I of the appendix. Comparing the functionals, we find that the two pure GGAs, revPBE⁴⁷ and PBE,⁴⁶ (indicated by plain grey bars) significantly underestimate the PT barriers. For systems with low PT barriers, underestimating barriers can give qualitatively incorrect results. For instance, in the case of the malonaldehyde (system 1 in Fig. 1), PBE predicts 8 meV far less than the reference value of 168 meV. PBE0, which mixes in 25% Fock exchange with the PBE exchange,¹⁵ improves the PT barriers. The meta-GGA SCAN is overall more accurate than PBE, but less accurate than PBE0. Despite the fact that dispersion forces contribute to hydrogen bonding, adding dispersion corrections at the DFT-D3²³ or at the TS²⁰ level to PBE has almost no impact on the predicted PT barrier. Interestingly, a similar insensitivity is also exhibited with the inclusion of rVV10 non-local correlation corrections to SCAN.⁴⁹ In contrast, several vdW-DFs, in particular vdW-DF-cx,^{29,30} vdW-DF,²⁶ and vdW-DF2²⁷ have significantly smaller deviations from the reference than the GGAs. The most accurate non-hybrid functional is vdW-DF2 with a mean absolute deviation (MAD) of 0.073 eV, only a quarter of that of PBE of 0.279 eV. In comparison, the MAD of PBE0 is 0.094 eV. The reduced deviation of vdW-DF can be traced to the GGA gradient correlations having a larger negative contribution to the barrier than the fully non-local vdW-DF correlation. For instance, going from revPBE to vdW-DF, which keeps the exchange fixed, causes MAD to drop from 0.226 eV to 0.104 eV. As both of the non-local correlation and hybrid exchange increase PT barriers, the most accurate functional is obtained with the hybrid vdW-DF-cx with 20% Fock exchange (vdW-DF-cx0-20),^{40,41} with a MAD of 0.037 eV, while the variant using 25% Fock exchange (vdW-DF-cx0) gives a MAD of 0.053 eV. Finally, we note the empirical B3LYP functional,¹⁶ which also uses 20% Fock exchange and a reduced GGA correlation (0.81 LYP⁶³) also provides accurate PT barriers, with a MAD of 0.041 eV.

Fig. 4 shows the individual correlation components for eight different functionals for the PT barrier of the formic acid dimer. It shows how the non-local correlation contribution of vdW-DF reduces the PT barrier less than the GGA correlation, thus making vdW-DF and vdW-DF2 the most accurate functionals for this PT barrier. As noted before, the comparison is most evident when comparing revPBE and vdW-DF as the exchange is kept fixed. The D3 correction in PBE-D3 and the rVV10 non-local correlation contribution in SCAN-rVV10 are barely visible.

IV. ANALYSIS OF ENERGETIC CONTRIBUTIONS OF VDW-DF

The dramatically improved performance of vdW-DF and vdW-DF2 compared to the GGAs, and the excellent

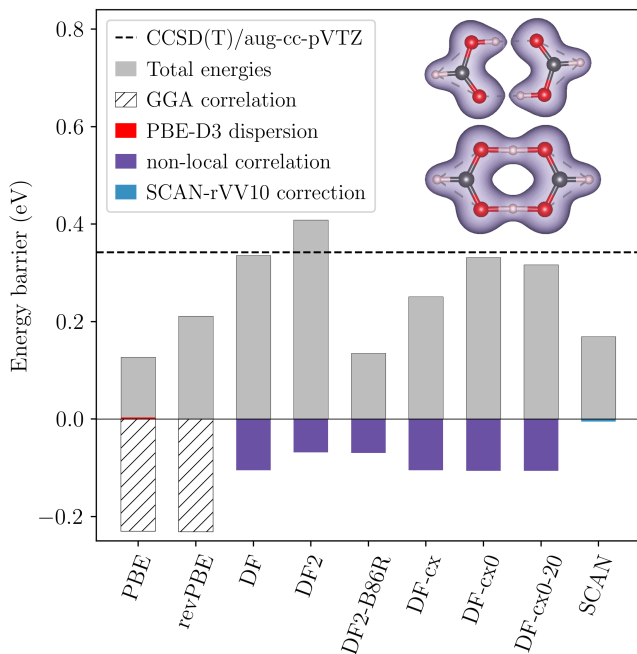


FIG. 4: Total energies and correlation components of the PT barrier for the formic acid dimer. The quantum chemical reference indicated with the dashed line.¹ The inset shows the density isosurfaces in the ground and transition state. The contributions of GGA correlation, non-local correlation with rVV10 and vdW-DF, and D3 corrections are indicated. The visualization in the inset and elsewhere is generated by VESTA.⁶⁴

performance of hybrid vdW-DF-cx prompted us to perform an analysis of the improved PT barriers. We retain the double-PT formic acid dimer (system 2 in Fig. 1) as a case study.

A. Exchange contribution

The degree of underestimation with GGAs as well as the performance of individual vdW-DF variants depends on the specific exchange functional used. Jenkins et al.⁶⁵ recently highlighted how the gradient component of the s -resolved exchange energy can be a useful tool to analyze why the choice of exchange enhancement factor $F_x(s)$ causes the performance of different vdW-DFs to differ for different types of systems. The GGA exchange itself is expressed as modulation of the LDA exchange, as follows

$$E_x^{\text{GGA}}[n] = \int d^3r n(\mathbf{r}) \epsilon_x^{\text{LDA}}(n(\mathbf{r})) F_x(s), \quad (2)$$

with the reduced gradient given by $s(\mathbf{r}) = |\nabla n(\mathbf{r})|/2(3\pi^2)^{1/3}n(\mathbf{r})^{4/3}$. In turn, the s -resolved

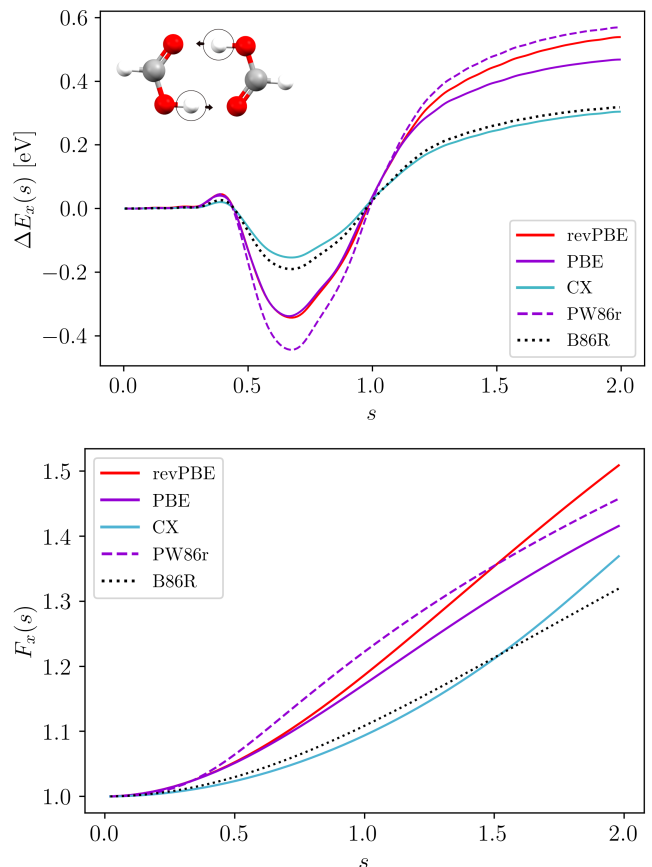


FIG. 5: s -integrated exchange barrier ($\Delta E_x(s)$) of the formic acid dimer for different selected exchange functionals (upper panel) and Corresponding enhancement factors (lower panel) plotted as a function of s .

exchange energy is given by

$$e_x(s) = \int d^3r n(\mathbf{r}) \epsilon_x^{\text{LDA}}(n(\mathbf{r})) [F_x(s) - 1] \delta(s - s(\mathbf{r})). \quad (3)$$

The contribution to the PT energy is given by the difference between the transition state (ts) and ground state (gs) as follows:

$$\Delta e_x(s) = e_x^{\text{ts}}(s) - e_x^{\text{gs}}(s). \quad (4)$$

The s -integrated exchange energy density is given by

$$\Delta E_x(s) = \int_0^s \Delta e_x(s') ds'. \quad (5)$$

Numerically, we computed Eq. 5 using the Savitzky–Golay⁶⁶ filter fitted with a third-degree polynomial to remove the noise imposed due to grid-point integration and then take the derivative to obtain Eq. 4.

The result is shown in Fig. 5. Note that this analysis only takes the explicit energetic contributions of

Eq. 3 into account, neglecting contributions from self-consistency which can be considerable.^{33,65} We can roughly discriminate two main s regions: $0.4 < s < 0.75$ which reduces the PT barrier, and $s > 0.75$ which increases the barrier. Comparing revPBE to PBE exchange, we can trace the larger PT barrier of the former, to the increasing difference between the values of $F_x(s)$ as s increases, and that most of the difference comes from regions with $s > 1.0$. It is also interesting that vdW-DF and vdW-DF2 end up with quite similar energies, even though the exchange functionals, revPBE and PW86r, differ considerably in shape. This result is due to a partial cancellation of positive and negative exchange contributions to the PT barrier. Comparing the enhancement factors, $F_x(s)$, (lower panel Fig. 5) with $\Delta E_x(s)$ reveals that the larger value of the PW86r $F_x(s)$ coincides with a larger slope of $\Delta E_x(s)$ in most of the negatively and positively-contributing s regions (top panel). The final difference also partially cancels with the small difference in non-local correlation contributions. With a MAD of 0.144 eV, vdW-DF-cx performs more accurately than vdW-DF2-B86R with a MAD of 0.254 eV. This result can be related both to slightly smaller values of $F_x(s)$ in the regime that contributes to lowering the barrier, as well as considerably larger values beyond $s > 1.0$. The full effect of this is partly counteracted by self consistency which influences the kinetic energy considerably in Fig. 5. Tab. I shows that while several vdW-DFs perform better than GGAs, not all vdW-DFs are equally accurate. For instance, PBE performs better than the recently developed vdW-DF3 variants; however, this is not due to the non-local correlation, but rather their “soft” exchange functionals, i.e. the $F_x(s)$ shape has overall lower values. In fact, truly “soft” GGAs such as PBEsol⁶⁷ are even less accurate with a MAD of 0.4 eV. The “soft” form in the small-to-medium s -regime is crucial for making vdW-DF accurate for other classes of systems such as coinage metals and layered systems.^{30,33,36,68} In this sense, it is encouraging that vdW-DF-cx, which can be labeled “soft”, performs relatively well. Moreover, the most accurate functionals are the hybrid variants of vdW-DF-cx, in line with accurate results found for other chemical reactions.^{40,41}

B. Analysis of the role of non-local correlation

For analyzing vdW-DF, the local responsiveness $q_0(\mathbf{r})$ is the most natural variable as it enters into the non-local correlation kernel $\phi(\mathbf{r}_1, \mathbf{r}_2) = \phi(D, \delta)$ through dimensionless parameters δ and D . In Sec. IV C, we will also project non-local correlation density onto $s(\mathbf{r})$, for sake of comparison with GGA correlation. The parameter δ is the relative difference in responsiveness $q_0(\mathbf{r})$ (inverse length scale) of two density regions

$$\delta = \frac{|q_0(\mathbf{r}_1) - q_0(\mathbf{r}_2)|}{q_0(\mathbf{r}_1) + q_0(\mathbf{r}_2)}, \quad (6)$$

and the effective dimensionless separation D is given by

$$D = \frac{1}{2} (q_0(\mathbf{r}_1) + q_0(\mathbf{r}_2)) |\mathbf{r}_1 - \mathbf{r}_2|. \quad (7)$$

The parameter $q_0(\mathbf{r})$ is, within vdW-DF, given by

$$q_0(\mathbf{r}) = \left(\frac{\epsilon_c^{\text{LDA}}}{\epsilon_x^{\text{LDA}}} + 1 - \frac{Z_{\text{ab}}}{9} s(\mathbf{r})^2 \right) k_{\text{F}}(\mathbf{r}), \quad (8)$$

where $k_{\text{F}}(\mathbf{r})$ is the local Fermi vector. Z_{ab} is equal to -0.849 for vdW-DF1 and vdW-DF3-opt1 and -1.887 for vdW-DF2 and vdW-DF3-opt2. The spatial non-local correlation density is given by

$$e_c^{\text{nl}}(\mathbf{r}) = \frac{n(\mathbf{r})}{2} \int d^3\mathbf{r}' n(\mathbf{r}') \phi(\mathbf{r}, \mathbf{r}'), \quad (9)$$

and, subsequently, the q_0 -resolved non-local correlation can be defined as

$$e_c^{\text{nl}}(q_0) = \int d^3r e_c^{\text{nl}}(\mathbf{r}) \delta(q_0 - q_0(\mathbf{r})). \quad (10)$$

The q_0 -resolved non-local correlation contribution to the PT barrier is then given as

$$\Delta e_c^{\text{nl}}(q_0) = e_c^{\text{nl,ts}}(q_0) - e_c^{\text{nl,gs}}(q_0), \quad (11)$$

and the corresponding q_0 -integrated non-local correlation barrier is

$$\Delta E_c^{\text{nl}}(q_0) = \int_0^{q_0} \Delta e_c^{\text{nl}}(q_0') dq_0'. \quad (12)$$

For the analysis of the non-local correlation contributions to PT barriers, Fig. 6 shows four interlinked panels. Panel (a) shows three selected q_0 isosurfaces for the ground state (gs) and transition state (ts). The overlaid contours indicate the non-local correlation density as given by Eq. 9. The three isosurfaces ($q_0 \approx 1.2, 1.8,$ and 2.2) were determined from the q_0 -resolved non-local correlation of Eq. 10 of the ground and transition states provided in panel (c), with the difference provided in panel (d). The rulers indicate the $D = 3$ separation, as well the physical lengths of 2 a.u. (Bohr). Panel (b) shows the vdW-DF kernel. The upper left isosurface of panel (a) for $q_0 \approx 1.2$ coincides with fairly low density regions, except for the regions directly between hydrogens and its oxygen neighbour in the adjacent molecule. Thus, this positive contribution to the non-local correlation of the ground state causes a lowering of the PT barrier. The larger blue isosurfaces around the void in between the two molecules for the transition state also contribute somewhat to lowering the PT barrier. This contribution can be viewed as a long-range dispersion effect as the distance from one to the other end of the void coincides with $D \approx 3$, i.e. the minimum of the kernel (b). The isosurfaces corresponding to $q_0 \approx 1.8$ (mid panels (a)) show additional lobes around the hydrogen atoms in the

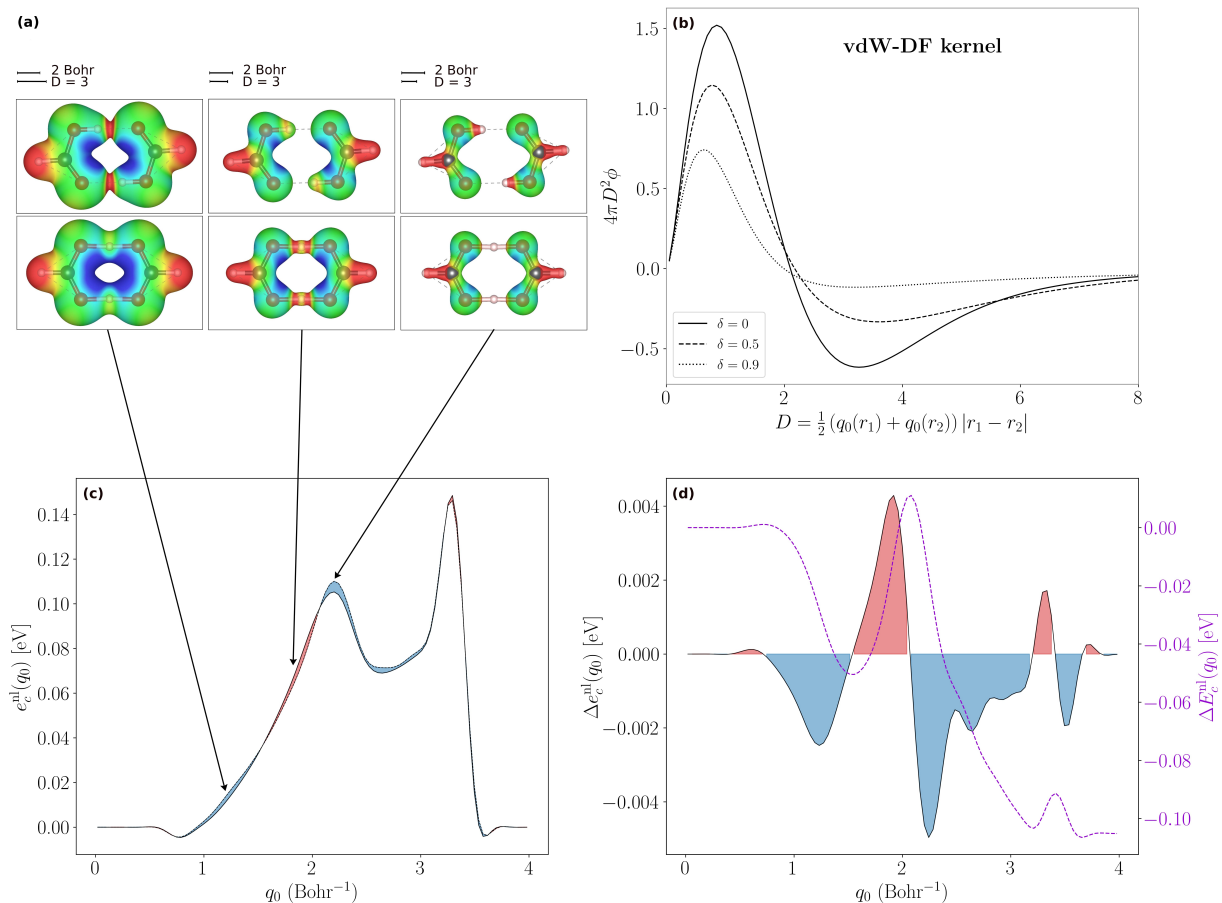


FIG. 6: Non-local correlation contributions to the double PT transfer energy in formic acid: **(a)** q_0 -isosurfaces with $q_0 \approx 1.2, 1.8,$ and 2.2 (atomic units) overlaid by non-local correlation density $e_c^{nl}(\mathbf{r})$ (Eq. 9). Red indicates negative contributions and blue positive. The upper rulers indicate physical lengths of 2 Bohr (i.e. 2 atomic units) $2 \text{ Bohr} \approx 1.06 \text{ \AA}$, and the lower unit-less scaled lengths of $D = 3$ entering into the vdW-DF kernel,²⁶ depicted for reference in panel **(b)**. Panel **(c)** shows the total non-local correlation (Eq. 10) of the ground and the transition state. Blue shading indicates negative net contributions to the PT barrier and red indicates net positive contributions. Panel **(d)** shows the corresponding q_0 -resolved contributions to the PT barrier while the dashed curve shows the integrated contributions.

transition state, while the ground state isosurface has been disconnected. These isosurfaces differences explain the increase in the positive non-local correlation energy of the transition state, thus increasing the magnitude of the PT barrier. Finally, the upper right isosurface corresponds to $q_0 = 2.2$ in which the isosurface lobes around the hydrogen in the transition state has vanished, but the isosurfaces around the hydrogen in the ground state cause a significant reduction of the PT barrier. At this value of q_0 , the effective separation D has contracted significantly causing intra-molecular correlation to be dominating contribution.

C. Reduced-gradient resolved correlation comparison

The previous subsection highlighted the utility of analyzing vdW-DF in terms of the spatial distribution of $q_0(\mathbf{r})$ which enters into the kernel $\phi(D, \delta)$ of vdW-DF. In GGA correlation,⁴⁶ a key variable is the reduced gradient $t = |\nabla n(\mathbf{r})|/2k_s(\mathbf{r})n(\mathbf{r})$, which is defined using Thomas-Fermi screening length $k_s = \sqrt{4k_F/\pi}$. In terms of t , the total PBE correlation energy can be expressed

$$E_c^{\text{PBE}} = \int d^3r n(\mathbf{r}) [\epsilon_c^{\text{LDA}}(\mathbf{r}) + H(n(\mathbf{r}), t(\mathbf{r}))], \quad (13)$$

where H is the gradient contribution function. In order to analyze the effect of correlation and exchange on an equal footing, whether at the GGA or vdW-DF level, we benefit from resolving these quantities onto the same

variable. We here choose the reduced gradient s which was used for exchange in Fig. 5. The corresponding s -resolved differential PBE correlation energy is given by

$$e_c^{\text{PBE}}(s) = \int d^3r n(\mathbf{r}) H(r, t(s)) \delta(s - s(\mathbf{r})), \quad (14)$$

with the corresponding integrated quantity given by

$$\Delta E_c^{\text{PBE}}(s) = \int_0^s \Delta e_c^{\text{PBE}}(s') ds'. \quad (15)$$

The projection of vdW-DF onto s is similar to Eq. 10. Fig. 7 shows the result for the PT energy barrier contribution $\Delta E_c^{\text{PBE}}(s)$ and the non-local correlation. Comparing the curves with the exchange part of Fig. 5 shows that the curve bear some resemblance, but with opposite prefactor and earlier onset of correlation contribution than exchange with increasing s . Comparing GGA and vdW-DF correlation shows that while the shapes are similar, the former has much larger positive and negative contributions beyond $s \approx 0.4$. Moreover beyond $s \approx 1.5$, vdW-DF correlation flattens, while the magnitude of GGA correlation continues to grow. Inspecting the isosurfaces, we found that the large $s > 1$ values corresponds to large isosurfaces similar to the low q_0 values.

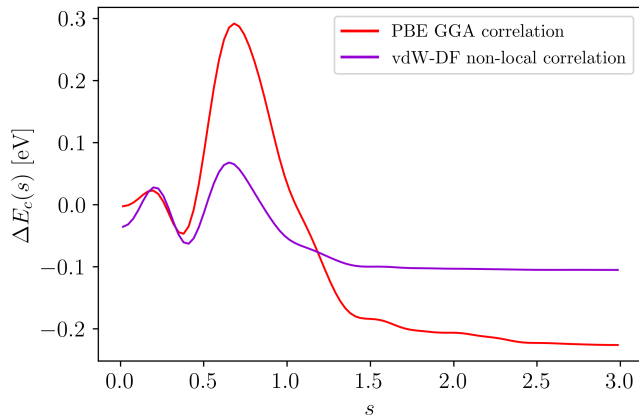


FIG. 7: s -resolved gradient component of the PBE correlation PT barrier and vdW-DF non-local correlation are plotted as function of s .

V. CONCLUSIONS AND OUTLOOK

We have compared and analyzed the performance of different functionals for proton-transfer energy barriers and found that using non-local correlation in vdW-DF rather than GGA correlation causes a non-intuitive lowering of the energy barriers, typically improving accuracy compared to GGA, which tends to underestimate energy barriers. The best performance was provided by a hybrid version of the consistent-exchange van der Waals density functional vdW-DF-cx with 20% Fock exchange.

The improved PT transfer barriers of vdW-DF is highly encouraging because these functional can account for dispersion forces responsible for the cohesion of many proton-transfer systems. Beyond this, our study points to the possibility that the usage of a non-local kernel reflects a true geometry-sensitive repulsive short-range correlation contribution. In this context, we emphasize that while vdW-DF was designed with dispersion forces in mind, the theory is rooted in exact constraints and many-body theory and therefore is not limited to long range dispersion forces as such. vdW-DF is a true non-local correlation functional with contributions both at short and long ranges. At the same time, the performance of approximative exchange-correlation functionals are generally contingent on the various simplifications and parametrizations used in their construction. The improved performance may also be a mostly “fortuitous” effect arising due to typically smaller semi-local correlation-type effects in vdW-DF. Exploring this question merits further theoretical and computational investigations and may pave the way for more accurate methods using non-local functionals for improving chemical reaction energies.

ACKNOWLEDGMENTS

The computations of this work were carried out on UNINETT Sigma2 high performance computing resources (grant NN9650K). This work is supported by the Research Council of Norway as a part of the Young Research Talent project FOX (302362). We thank Rasmus Tranås and Elin Dypvik Sødahl for comments. KB acknowledges discussions with T. Jenkins and T. Thonhauser on visualization.

Appendix A: Tabulated data for PT14 set

Table I shows the computed data for all studied functionals. The upper part shows results for all but the vdW-DFs, which is shown in the lower part.

TABLE I: PT energy barriers, mean absolute deviations (MAD), mean deviations (MD), mean absolute relative deviation (MARD), and mean relative deviations (MRD) for the PT14 benchmarking set for different density functionals. The units are in electronvolts (eV).

Systems	Ref.	PBE	PBE-D3	PBE-TS	revPBE	PBE0	SCAN	SCAN-rVV10	rVV10	B3LYP	B3LYP-D3	PBEsol
1	0.168	0.008	0.015	0.009	0.049	0.073	0.038	0.036	0.073	0.130	0.144	-0.079
2	0.343	0.127	0.130	0.130	0.211	0.207	0.160	0.155	0.208	0.289	0.289	-0.029
3	2.028	1.814	1.818	1.813	1.865	1.999	1.950	1.948	1.925	2.080	2.087	1.692
4	0.828	0.655	0.657	0.650	0.762	0.755	0.707	0.699	0.780	0.885	0.886	0.451
5	1.650	1.328	1.326	1.324	1.369	1.540	1.472	1.471	1.406	1.589	1.587	1.228
6	1.594	1.347	1.352	1.348	1.391	1.536	1.446	1.445	1.434	1.597	1.606	1.242
7	1.570	1.271	1.272	1.271	1.319	1.467	1.408	1.406	1.348	1.520	1.521	1.163
8	2.643	2.254	2.255	2.254	2.287	2.495	2.408	2.406	2.351	2.559	2.562	2.152
9	2.061	1.778	1.778	1.776	1.832	1.973	1.925	1.923	1.881	2.046	2.045	1.654
10	2.848	2.509	2.510	2.508	2.544	2.741	2.673	2.670	2.625	2.818	2.820	2.403
11	3.523	3.144	3.144	3.147	3.174	3.472	3.370	3.368	3.224	3.524	3.523	3.060
12	1.388	1.171	1.178	1.172	1.237	1.338	1.265	1.262	1.270	1.435	1.448	1.037
13	1.256	0.987	0.991	0.986	1.052	1.158	1.089	1.087	1.078	1.248	1.254	0.854
14	2.55	2.150	2.156	2.152	2.200	2.387	2.298	2.295	2.251	2.487	2.498	2.025
MD	–	-0.279	-0.276	-0.279	-0.225	-0.094	-0.160	-0.163	-0.185	-0.017	-0.013	-0.399
MAD	–	0.279	0.276	0.279	0.225	0.094	0.160	0.163	0.185	0.040	0.040	0.399
MRD %	–	-24.8	-24.3	-24.8	-18.3	-11.2	-16.9	-17.3	-15.4	-2.8	-2.0	-38.3
MARD %	–	24.8	24.3	24.8	18.3	11.2	16.9	17.3	15.4	4.7	4.2	38.3

Systems	Ref.	DF	DF2	DF-cx	DF-cx0	DF-cx0-20	DF2-B86R	DF2-B86R0	DF2-B86R0-20	DF-optB88	DF-optPBE	DF3-opt1	DF3-opt2
1	0.168	0.131	0.188	0.089	0.156	0.143	0.016	0.101	0.084	0.042	0.068	-0.028	0.005
2	0.343	0.336	0.409	0.251	0.333	0.317	0.135	0.252	0.229	0.173	0.225	0.054	0.114
3	2.028	2.003	2.088	1.951	2.143	2.106	1.850	2.064	2.022	1.893	1.918	1.787	1.833
4	0.828	0.930	1.032	0.822	0.926	0.906	0.686	0.832	0.803	0.723	0.788	0.574	0.657
5	1.650	1.501	1.571	1.459	1.675	1.633	1.354	1.590	1.544	1.406	1.427	1.305	1.344
6	1.594	1.514	1.588	1.470	1.664	1.626	1.371	1.584	1.110	1.418	1.438	1.317	1.358
7	1.570	1.446	1.517	1.397	1.599	1.561	1.283	1.508	1.464	1.344	1.366	1.232	1.270
8	2.643	2.425	2.523	2.392	2.640	2.592	2.282	2.552	2.500	2.345	2.351	2.232	2.268
9	2.061	1.973	2.057	1.919	2.121	2.082	1.803	2.031	1.987	1.860	1.885	1.744	1.787
10	2.848	2.679	2.782	2.644	2.886	2.839	2.547	2.808	2.757	2.599	2.605	2.495	2.531
11	3.523	3.301	3.382	3.269	3.609	3.542	3.183	3.549	3.477	3.237	3.237	3.147	3.172
12	1.388	1.391	1.476	1.323	1.500	1.465	1.201	1.404	1.364	1.261	1.289	1.132	1.181
13	1.256	1.209	1.297	1.143	1.324	1.289	1.006	1.217	1.175	1.079	1.108	0.941	0.988
14	2.55	2.361	2.471	2.310	2.560	2.511	2.173	2.462	2.406	2.253	2.268	2.110	2.154
MD	–	-0.089	-0.005	-0.144	0.049	0.012	-0.254	-0.035	-0.078	-0.201	-0.177	-0.315	-0.271
MAD	–	0.104	0.073	0.144	0.053	0.037	0.254	0.047	0.078	0.201	0.177	0.315	0.271
MRD %	–	-5.0	3.3	-11.6	2.6	-0.2	-23.0	-5.9	-9.3	-18.3	-14.7	-29.8	-24.8
MARD %	–	6.8	6.5	11.6	3.9	3.7	23.0	6.6	9.3	18.3	14.7	29.8	24.8

- [1] G. F. Mangiatordi, E. Brémond, and C. Adamo, “DFT and proton transfer reactions: A benchmark study on structure and kinetics”, *J. Chem. Theory Comput.* **8**, 3082 (2012).
- [2] A. Karton, R. J. O’Reilly, and L. Radom, “Assessment of theoretical procedures for calculating barrier heights for a diverse set of water-catalyzed proton-transfer reactions”,

- J. Phys. Chem. A* **116**, 4211 (2012).
- [3] S. Y. Reece and D. G. Nocera, “Proton-coupled electron transfer in biology: Results from synergistic studies in natural and model systems”, *Annu. Rev. Biochem.* **78**, 673 (2009).
- [4] D. Jacquemin, J. Zúñiga, A. Requena, and J. P. Céron-Carrasco, “Assessing the importance of proton transfer

- reactions in DNA”, *Acc. Chem. Res.* **47**, 2467 (2014).
- [5] Joanna S. Stevens et. al., “Proton transfer and hydrogen bonding in the organic solid state: a combined XRD/XPS/ssNMR study of 17 organic acid–base complexes”, *Phys. Chem. Chem. Phys.* **16**, 1150 (2014).
- [6] S. Horiuchi, S. Ishibashi, and Y. Tokura, “3 - Hydrogen-bonded organic molecular ferroelectrics/antiferroelectrics”, in *Organic Ferroelectric Materials and Applications*, Woodhead Publishing Series in Electronic and Optical Materials, edited by K. Asadi (Woodhead Publishing, 2022) pp. 47–84.
- [7] Sachio Horiuchi et. al., “Above-room-temperature ferroelectricity in a single-component molecular crystal”, *Nature* **463**, 789 (2010).
- [8] S. Horiuchi, K. Kobayashi, R. Kumai, and S. Ishibashi, “Proton tautomerism for strong polarization switching”, *Nat. Commun.* **8** (2017).
- [9] W. Kohn and L. J. Sham, “Self-consistent equations including exchange and correlation effects”, *Phys. Rev.* **140**, A1133 (1965).
- [10] J. P. Perdew, “Density-functional approximation for the correlation energy of the inhomogeneous electron gas”, *Phys. Rev. B* **33**, 8822 (1986).
- [11] A. D. Becke, “Density-functional exchange-energy approximation with correct asymptotic behavior”, *Phys. Rev. A* **38**, 3098 (1988).
- [12] V. Barone, L. Orlandini, and C. Adamo, “Proton transfer in model hydrogen-bonded systems by a density functional approach”, *Chem. Phys. Lett.* **231**, 295 (1994).
- [13] A. D. Becke, “A new mixing of hartree–fock and local density-functional theories”, *J. Chem. Phys.* **98**, 1372 (1993).
- [14] A. Pribram-Jones, D. A. Gross, and K. Burke, “DFT: A theory full of holes?”, *Annu. Rev. Phys. Chem.* **66**, 283 (2015).
- [15] C. Adamo and V. Barone, “Toward reliable density functional methods without adjustable parameters: The pbe0 model”, *J. Chem. Phys.* **110**, 6158 (1999).
- [16] A. D. Becke, “Density-functional thermochemistry. iii. the role of exact exchange”, *J. Chem. Phys.* **98**, 5648 (1993).
- [17] J. L. Bao, L. Gagliardi, and D. G. Truhlar, “Self-interaction error in density functional theory: An appraisal”, *J. Phys. Chem. Lett.* **9**, 2353 (2018).
- [18] S. Patchkovskii and T. Ziegler, “Improving “difficult” reaction barriers with self-interaction corrected density functional theory”, *J. Chem. Phys.* **116**, 7806 (2002).
- [19] T. Tsuneda and K. Hirao, “Self-interaction corrections in density functional theory”, *J. Chem. Phys.* **140**, 18A513 (2014).
- [20] A. Tkatchenko and M. Scheffler, “Accurate molecular van der waals interactions from ground-state electron density and free-atom reference data”, *Phys. Rev. Lett.* **102**, 073005 (2009).
- [21] S. Grimme, “Accurate description of van der waals complexes by density functional theory including empirical corrections”, *J. Comput. Chem.* **25**, 1463 (2004).
- [22] S. Grimme, “Semiempirical GGA-type density functional constructed with a long-range dispersion correction”, *J. Comput. Chem.* **27**, 1787 (2006).
- [23] S. Grimme, J. Antony, S. Ehrlich, and H. Krieg, “A consistent and accurate ab initio parametrization of density functional dispersion correction (DFT-D) for the 94 elements h-pu”, *J. Chem. Phys.* **132**, 154104 (2010).
- [24] S. Grimme, “Density functional theory with london dispersion corrections”, *WIREs Comput. Mol. Sci.* **1**, 211 (2011).
- [25] M. Stöhr, T. V. Voorhis, and A. Tkatchenko, “Theory and practice of modeling van der waals interactions in electronic-structure calculations”, *Chem. Soc. Rev.* **48**, 4118 (2019).
- [26] M. Dion, H. Rydberg, E. Schröder, D. C. Langreth, and B. I. Lundqvist, “Van der waals density functional for general geometries”, *Phys. Rev. Lett.* **92**, 246401 (2004).
- [27] K. Lee, E. D. Murray, L. Kong, B. I. Lundqvist, and D. C. Langreth, “Higher-accuracy van der waals density functional”, *Phys. Rev. B* **82**, 081101 (2010).
- [28] I. Hamada, “Van der waals density functional made accurate”, *Phys. Rev. B* **89**, 121103 (2014).
- [29] K. Berland and P. Hyldgaard, “Exchange functional that tests the robustness of the plasmon description of the van der waals density functional”, *Phys. Rev. B* **89**, 035412 (2014).
- [30] Kristian Berland et. al., “Van der waals density functionals built upon the electron-gas tradition: Facing the challenge of competing interactions”, *J. Chem. Phys.* **140**, 18A539 (2014).
- [31] J. Klimeš, D. R. Bowler, and A. Michaelides, “Chemical accuracy for the van der waals density functional”, *J. Phys. Condens. Matter.* **22**, 022201 (2009).
- [32] Klimeš, Jiří, D. R. Bowler, and A. Michaelides, “Van der waals density functionals applied to solids”, *Phys. Rev. B* **83**, 195131 (2011).
- [33] D. Chakraborty, K. Berland, and T. Thonhauser, “Next-generation nonlocal van der waals density functional”, *J. Chem. Theory Comput.* **16**, 5893 (2020).
- [34] T. Thonhauser, V. R. Cooper, S. Li, A. Puzder, P. Hyldgaard, and D. C. Langreth, “Van der waals density functional: Self-consistent potential and the nature of the van der waals bond”, *Phys. Rev. B* **76** (2007).
- [35] Elsebeth Schröder et. al., “The vdW-DF family of non-local exchange-correlation functionals”, in *Non-Covalent Interactions in Quantum Chemistry and Physics* (Elsevier, 2017) pp. 241–274.
- [36] Kristian Berland et. al., “Van der waals forces in density functional theory: a review of the vdW-DF method”, *Rep. Prog. Phys.* **78**, 066501 (2015).
- [37] P. Hyldgaard, Y. Jiao, and V. Shukla, “Screening nature of the van der waals density functional method: a review and analysis of the many-body physics foundation”, *J. Phys. Condens. Matter.* **32**, 393001 (2020).
- [38] P. Hyldgaard, K. Berland, and E. Schröder, “Interpretation of van der waals density functionals”, *Phys. Rev. B* **90**, 075148 (2014).
- [39] K. Berland, D. Chakraborty, and T. Thonhauser, “Van der waals density functional with corrected C_6 coefficients”, *Phys. Rev. B* **99**, 195418 (2019).
- [40] Kristian Berland et. al., “Assessment of two hybrid van der waals density functionals for covalent and non-covalent binding of molecules”, *J. Chem. Phys.* **146**, 234106 (2017).
- [41] Y. Jiao, E. Schröder, and P. Hyldgaard, “Extent of fock-exchange mixing for a hybrid van der waals density functional?”, *J. Chem. Phys.* **148**, 194115 (2018).
- [42] O. A. Vydrov and T. Van Voorhis, “Nonlocal van der waals density functional: The simpler the better”, *J. Chem. Phys.* **133**, 244103 (2010).

- [43] R. Sabatini, T. Gorni, and S. de Gironcoli, “Nonlocal van der waals density functional made simple and efficient”, *Phys. Rev. B* **87**, 041108 (2013).
- [44] D. O. Lindroth and P. Erhart, “Thermal transport in van der waals solids from first-principles calculations”, *Phys. Rev. B* **94**, 115205 (2016).
- [45] I. Hamada, Y. Hamamoto, and Y. Morikawa, “Image potential states from the van der waals density functional”, *J. Chem. Phys.* **147**, 044708 (2017).
- [46] J. P. Perdew, K. Burke, and M. Ernzerhof, “Generalized gradient approximation made simple”, *Phys. Rev. Lett.* **77**, 3865 (1996).
- [47] Y. Zhang and W. Yang, “Comment on ‘generalized gradient approximation made simple’”, *Phys. Rev. Lett.* **80**, 890 (1998).
- [48] J. Sun, A. Ruzsinszky, and J. P. Perdew, “Strongly constrained and appropriately normed semilocal density functional”, *Phys. Rev. Lett.* **115**, 036402 (2015).
- [49] H. Peng, Z.-H. Yang, J. P. Perdew, and J. Sun, “Versatile van der waals density functional based on a meta-generalized gradient approximation”, *Phys. Rev. X* **6**, 041005 (2016).
- [50] G. Kresse and J. Hafner, “Ab initio molecular dynamics for liquid metals”, *Phys. Rev. B* **47**, 558 (1993).
- [51] G. Kresse and J. Furthmüller, “Efficiency of ab-initio total energy calculations for metals and semiconductors using a plane-wave basis set”, *Comput. Mater. Sci.* **6**, 15 (1996).
- [52] G. Kresse and J. Furthmüller, “Efficient iterative schemes for ab initio total-energy calculations using a plane-wave basis set”, *Phys. Rev. B* **54**, 11169 (1996).
- [53] P. Giannozzi et. al., “Advanced capabilities for materials modelling with quantum ESPRESSO”, *J. Phys. Condens. Matter.* **29**, 465901 (2017).
- [54] P. Giannozzi et. al., “Advanced capabilities for materials modelling with quantum ESPRESSO”, *J. Phys. Condens. Matter.* **29**, 465901 (2017).
- [55] J. Neugebauer and M. Scheffler, “Adsorbate-substrate and adsorbate-adsorbate interactions of na and k adlayers on al(111)”, *Phys. Rev. B* **46**, 16067 (1992).
- [56] D. R. Hamann, “Optimized norm-conserving vanderbilt pseudopotentials”, *Phys. Rev. B* **88** (2013).
- [57] Y. Jiao, E. Schröder, and P. Hyldgaard, “Signatures of van der waals binding: A coupling-constant scaling analysis”, *Phys. Rev. B* **97**, 10.1103/physrevb.97.085115 (2018).
- [58] A. M. Rappe, K. M. Rabe, E. Kaxiras, and J. D. Joannopoulos, “Optimized pseudopotentials”, *Phys. Rev. B* **41**, 1227 (1990).
- [59] S. Goedecker, M. Teter, and J. Hutter, “Separable dual-space gaussian pseudopotentials”, *Phys. Rev. B* **54**, 1703 (1996).
- [60] P. E. Blöchl, “Projector augmented-wave method”, *Phys. Rev. B* **50**, 17953 (1994).
- [61] G. Kresse and D. Joubert, “From ultrasoft pseudopotentials to the projector augmented-wave method”, *Phys. Rev. B* **59**, 1758 (1999).
- [62] M. e. a. Frisch, “Gaussian 09 (revision a02)”, Gaussian Inc. Wallingford CT (2009).
- [63] C. Lee, W. Yang, and R. G. Parr, “Development of the colle-salvetti correlation-energy formula into a functional of the electron density”, *Phys. Rev. B* **37**, 785 (1988).
- [64] K. Momma and F. Izumi, “VESTA 3 for three-dimensional visualization of crystal, volumetric and morphology data”, *J. Appl. Crystallogr.* **44**, 1272 (2011).
- [65] T. Jenkins, K. Berland, and T. Thonhauser, “Reduced-gradient analysis of van der waals complexes”, *Electron. Struct.* **3**, 034009 (2021).
- [66] A. Savitzky and M. J. E. Golay, “Smoothing and differentiation of data by simplified least squares procedures”, *Anal. Chem.* **36**, 1627 (1964).
- [67] G. I. e. a. Csonka, “Assessing the performance of recent density functionals for bulk solids”, *Phys. Rev. B* **79**, 155107 (2009).
- [68] F. Tran, L. Kalantari, B. Traoré, X. Rocquefelte, and P. Blaha, “Nonlocal van der waals functionals for solids: Choosing an appropriate one”, *Phys. Rev. Materials* **3**, 063602 (2019).